INORGANIC CHEMISTRY FRONTIERS

RESEARCH ARTICLE

View Article Online
View Journal

Cite this: DOI: 10.1039/d6qi00188b

Hypoxia active cyclometalated Ir(III) Nile red triplet photosensitisers

Judit Fodor, [a] Olga Mazuryk, *[b] Claire C. Condon, [a] Oriol Careta, [c] Amani B. Al Riyami, [a] Carme Nogués, [c] John J. Colleran, [d] Xiao Xiao,[e] Jianzhang Zhao [e] and Sylvia M. Draper *[a]

Cyclometalated Ir(III) compounds have gained increasing attention as promising photosensitisers for photodynamic therapy (PDT). Most photosensitisers exert their therapeutic effect by generating singlet oxygen through a light-activated reaction with molecular oxygen, which makes them less effective in treating hypoxic tumors. In this work, we report the synthesis, characterisation, photophysics, and biological studies of two novel, octahedral Ir(III) bis-cyclometalated photosensitisers, **[Ir-2ENR]$^+$** and **[Ir-3ENR]$^+$**, featuring an extended Nile red (NR) chromophore. The absorption and emission spectra of the complexes and their excited states are largely governed by the NR chromophore and lie within the biological window (650–800 nm) for excitation and application in PDT. Overall, **[Ir-3ENR]$^+$** displays more attractive photophysical properties, which is reflected in its higher photodynamic activity in SKBR-3 cells compared to its **2ENR**, and previously reported Ru(II), analogues. Further *in vitro* studies as reported here, using a MCF-7 cell line, examined the PDT effect under both normoxic and hypoxic conditions. The results revealed the excellent phototoxic activity of **[Ir-3ENR]Cl** (phototoxicity index = 179). This fluorescent mitochondria-accumulating complex, exerts its activity by combining type-I and type-II mechanisms and, more importantly, retains its cyto- and phototoxic activity under decreased oxygen concentrations. The data highlight how rational design can help overcome hypoxia limitation in conventional PDT and offer a promising approach to combat hypoxic solid tumors.

Received 27th January 2026,
Accepted 5th May 2026

DOI: 10.1039/d6qi00188b

rsc.li/frontiers-inorganic

Introduction

Photodynamic therapy (PDT) is a targeted, non-invasive approach to treat microbial infections, skin diseases and some types of cancer.[1] It often relies on the presence of oxygen and involves a non-toxic therapeutic agent or photosensitiser (PS), that is activated by light at a specific energy to produce $^1O_2$ or other reactive oxygen species (ROS), for the destruction of the target cells. Overall PDT seeks to accomplish the direct, controlled and localised damage of diseased or cancerous tissue *via* light activation. It offers the potential to achieve more specific cancer treatments and to address the multiple challenges arising from cancer cell resistance and unwanted side effects.[2]

The generation of ROS through light-activation of PS can occur *via* two different routes, type-I and type-II, that were originally distinguished by Gollnick[3] and Schenk[4] and further refined by Christopher Foote.[5] In type-I, the excited photosensitiser reacts with the solvent or substrate leading to radicals or radical ions and in type-II, the PS reacts with triplet oxygen to produce singlet oxygen.[5] Type-I is favourable over type-II in oxygen depleted tissues such as those found in bacterial infection sites or in cancer tumour environments.[6,7] Type-I PDT occurs *via* an electron transfer process involving O_2 and H_2O substrates. It results in the formation of ROS such as superoxide anion, $O^{2\bullet-}$, hydroxy radical, $^\bullet OH$, and hydrogen peroxide, H_2O_2.[8] ROS are normally generated in cells and the oxidant–antioxidant balance is usually maintained by cellular mechanisms.[9] PDT-generated oxidative phototoxicity leads to the over-production of ROS and cell death by either apoptosis or necrosis. It can also trigger inflammation-mediated immune responses and vascular damage.[10] A recent addition to PDT is the type-III mechanism. This and photocatalytic therapy (PACT) are independent of oxygen and work by directly targeting biomolecules.[11–13]

[a]*School of Chemistry, Trinity College Dublin, College Green, Dublin 2, Ireland. E-mail: smdraper@tcd.ie*
[b]*Department of Inorganic Chemistry, Faculty of Chemistry, Jagiellonian University, Gronostajowa 2, 30-387 Krakow, Poland. E-mail: olga.mazuryk@uj.edu.pl*
[c]*Departament de Biologia Cellular, Fisiologia i Immunologia, Universitat Autònoma de Barcelona, E-08193 Bellaterra, Barcelona, Spain*
[d]*Central Quad Grangegorman, School of Chemical and Pharmaceutical Sciences, Technological University Dublin, Dublin 7, D07 H6K8 Dublin, Ireland*
[e]*State Key Laboratory of Fine Chemicals, Frontier Science Centre for Smart Materials, Dalian University of Technology, E208 Western Campus, 2 Ling-Gong Road, Dalian 116012, P. R. China*

Ir(III) bis-cyclometalated compounds are excellent photosensitisers that have the ability to target crucial cellular proteins, lysosomes,[14,15] endoplasmic reticulum[16,17] and due to their charge and their high lipophilicity they often accumulate in the mitochondria and lead to mitochondrial dysfunction,[14,15,17–22] and can oxidise NADH.[20,21] Furthermore, cancer cells are more abundant in lipophilic charged molecules increasing the uptake of similar compounds into diseased cells.[23]

Two-photon activated Ir(III) photosensitisers have achieved remarkable $^1O_2$ quantum yields (92%);[24] large phototherapeutic effects (phototherapeutic index PI >885 and >1234 against malignant melanoma and non-small-cell lung cancer, respectively) and *in vivo* tumour growth inhibition (85%);[18] and an endoperoxide Ir(III) prodrug was able to synergistically release a highly cytotoxic Ir(III) complex, singlet oxygen, and an alkoxy radical upon two-photon excitation.[25]

In recent years the focus has shifted to designing Ir(III) compounds to enhance type I activity that is less reliant on the intracellular oxygen concentration and thereby avoid reduced photoactivity under hypoxic conditions.[12,15,21,26–38] The strategies in complex design generally involve donor–acceptor ligands;[24] binuclear compounds and a chromophore/fluorophore approach.[12,26,39] Despite significant developments many of the tested complexes have short comings, such as a low phototoxicity index[14,15,19,20] that decreases under hypoxic conditions,[21,29–31] require activation in the visible region (500 nm),[15,17,20,22,26–28,39,40] possess low solubility or need encapsulation (@PEG).[26,32]

Our group previously reported efficient Ru(II) and Ir(III) PSs functionalised with pyrene, BODIPY, carbazole, coumarin-6, Nile red, mono- and dinuclear complexes and multinuclear compounds with porphyrins.[33,34,41–46] Recently, we reported two heteroleptic Ru(II) bipyridyl transition metal (TM) based PSs, **[Ru-2ENR]Cl$_2$** and **[Ru-3ENR]Cl$_2$**, incorporating an appended Nile red lysochrome in a bid to aid lipophilicity and efficacy for application in PDT (Scheme 1a).[47,48] These complexes had two weakly emissive states originating from an intraligand charge transfer, ^{1}ILCT* (557/565 nm), and a metal to ligand charge transfer, ^{3}MLCT* (450 nm) transition. In addition, the more active **[Ru-3ENR](PF$_6$)$_2$** had a long lived, ILCT based, non-emissive triplet excited state (τ_T) of 234.7 μs (λ_{ex} 550 nm) that facilitates excellent $^1O_2$ generation (λ_{ex} 610 nm, Φ_Δ 90.4%). Both complexes had significant dark cytotoxicity (against human breast cancer SKBR-3 cell line) and the chloride salt of **[Ru-3ENR]$^{2+}$** reduced viability of 60% of the SKBR-3 cells at 10 nM concentrations after 630 nm excitation. Encouraged by the excellent photophysical properties and the promising biological behaviour of the **ENR** chromophore we set out to generate the Ir(III) analogues, with the aim of improving the photodynamic activity and cellular uptake. Following a fluorophore attachment design approach an ethynyl linker is found to tune the excited state properties: red-shift the absorption and promote ILCT and intraligand fluorescence.[33,34,47]

Herein we report the synthesis, characterisation and biological studies of two novel Ir(III) Nile red photosensitisers (Scheme 1b and c). The photodynamic activity of the compounds was tested on human breast cancer epithelial cells (SKBR-3) through dark and light-activated toxicity measurements. Detailed studies to explore the mechanism of cyto- and phototoxicity under normoxic and hypoxic conditions were performed on MCF-7 cells using the more effective **[Ir-3ENR]Cl.**

Impressively, this mitochondria-accumulating Ir complex showed excellent cyto-and phototoxic activity (on activation by 630 nm and 520 nm light) and its activity was enhanced under hypoxic conditions making it unusual in comparison to known type I PDT agents.

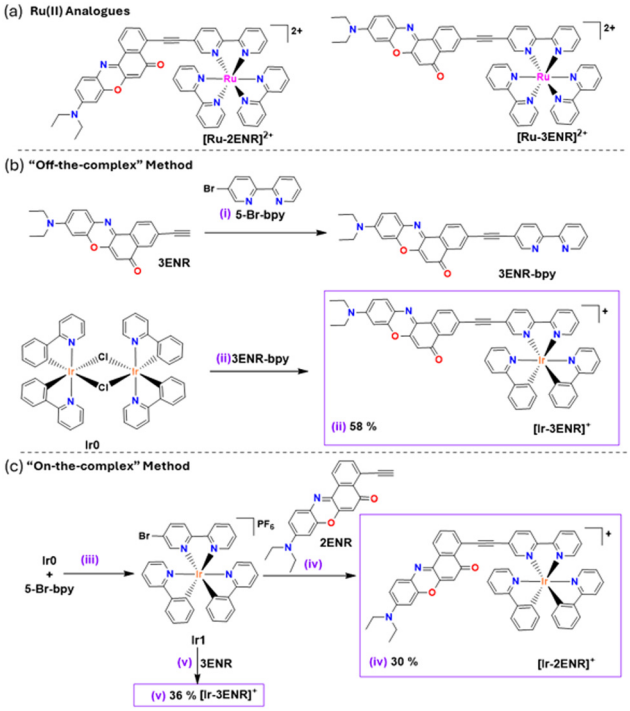

Scheme 1 (a) Ruthenium(II) analogues **[Ru-2ENR]$^{2+}$** and **[Ru-3ENR]$^{2+}$**; (b) "Off-the-complex" synthesis of **[Ir-3ENR]PF$_6$** (i) **3ENR** and 5-Br-2,2′-bipyridyl (1.5 equiv.), Pd(PPh$_3$)$_4$ (10 mol%), MeCN/Et$_3$N, 80 °C, 20 h, 17%; (ii) **Ir0**, **3ENR-bpy** (2.0 equiv.) CHCl$_3$, 60 °C, 4 h, counterion metathesis with KPF$_6$, 58%. (c) "On-the-complex" synthesis of **[Ir-2ENR]PF$_6$** and **[Ir-3ENR]PF$_6$** (iii) **Ir0**, 5-Br-2,2′-bipyridyl (2.0 equiv.), CH$_2$Cl$_2$, 40 °C, 18 h, counterion metathesis with KPF$_6$, 73%; (iv) **Ir1**, **2ENR** (2.5 equiv.), Pd(PPh$_3$)$_4$ (10 mol%), MeCN, Et$_3$N, 80 °C, 24 h, 30%; (v) **Ir1**, **3ENR** (2.0 equiv.) CHCl$_3$, 60 °C, 4 h, 36%.

Results and discussion

Synthesis

Two synthetic pathways: 'off-the-complex' and 'on-the-complex' were employed for the preparation of the heteroleptic Ir(III) phenylpyridine (ppy) complexes, incorporating NR-appended bipyridyl (bpy) ligands, **[Ir-2ENR]PF$_6$** and **[Ir-3ENR]PF$_6$**, (where **2ENR** = 2-ethynyl-9-(diethylamino)-5*H*-benzo[*a*]phenoxazin-5-one; **3ENR** = 3-ethynyl-9-(diethylamino)-5*H*-benzo[*a*]phenoxazin-5-one) (Scheme 1). In the 'off-the-complex' approach the extended ligand **3ENR-bpy** was prepared by Sonogashira[49] cross coupling of the **3ENR** moiety

with 5-Br-bpy and subsequently reacted, with the μ-chlorido-bridged Ir(III) dimer[50–52] (**Ir0**) (Scheme 1b). The low yield (17%) and poor solubility of the **3ENR-bpy** ligand made this route challenging so both complexes were prepared using an "on-the-complex" method, where the **2ENR** and **3ENR** chromophores were cross coupled to the yellow octahedral complex **Ir1** [53] to yield **[Ir-2ENR]PF_6** and **[Ir-3ENR]PF_6** as dark purple solids (30% and 36% yields respectively) (Scheme 1c). The successful formation and purification of **3ENR-bpy**, **[Ir-2ENR]PF_6** and **[Ir-3ENR]PF_6** were confirmed *via* HRMS and nuclear magnetic resonance (NMR) spectroscopy (Table S1 and Fig. S1–S5). The two complexes have unsymmetrical structures resulting in individual signals for all the protons in the aromatic region and complicating the ^{1}H and ^{13}C NMR spectra. Analysis of the chemical shifts and assignments can be found in the SI.

For the biological studies the complexes were converted to their chloride salts as these are more soluble in aqueous media. Anion exchange was achieved *via* silica column chromatography using a KCl eluent (CH_3CN, H_2O, KCl(aq), 100 : 10 : 1 v/v/v). Purity and complete anion exchange were confirmed *via* ^{35}Cl and ^{19}F NMR spectra (Fig. S6–S9).

Steady-state UV-vis absorption and emission studies

The UV-visible absorption spectra of **[Ir-2ENR]PF_6/Cl** and **[Ir-3ENR]PF_6/Cl** recorded in acetonitrile (MeCN) exhibit bands that are characteristic of cationic heteroleptic iridium(III) complexes. The high energy, intense bands are attributed to spin-allowed ligand centred (^{1}LC) π–π* transitions of ppy and bpy ligands (Fig. 1a and b). The bands and shoulders between 300–440 nm were ascribed to spin-allowed charge transfer (CT) bands, a combination of metal-to-ligand charge transfer (^{1}MLCT) and ligand-to-ligand charge transfer (^{1}LLCT) transitions.[54] The bands between 440 nm and 700 nm for the complexes were assigned to NR-centred ^{1}ILCT, with **[Ir-3ENR]PF_6** exhibiting the highest molar extinction coefficient (ε) in MeCN only and with the Cl counter ion red-shifting this transition (MeCN). The absorption of **3ENR** complexes were red shifted compared to their **2ENR** analogues in MeCN, due to increased conjugation and the ^{1}MLCT presented as a shoulder (Table S4). Assignments were made based on comparison to the spectra of the Ru(II) analogues, **[Ru-2ENR]$(PF_6)_2$**, **[Ru-3ENR]$(PF_6)_2$**, and the free **3ENR-bpy** ligand (Fig. S13a, b and Table 1).[47] The assignments for the new complexes also align with a detailed analyses of their electrochemical properties (see SI, Fig. S10–S12 and Table S2).

Solvent polarity had a significant influence on the NR-centred ^{1}ILCT transitions (Fig. 1c). These exhibited positive solvatochromism, blue-shifting the λ_{max} in the non-polar toluene (553 nm) compared to the polar methanol (581 nm), showing similar behaviour to the free **3ENR-bpy** ligand (Fig. S13, S14 and Tables S3, S4). As expected, the ^{1}MLCT absorption bands at *circa* 340 nm are less affected by solvent polarity (Table S5). The ^{1}ILCT absorption is more sensitive to the solvent environment in the Cl salts, where overall, we see more red-shifted absorption and higher extinction coefficients when in the same solvent (Fig. S11 and Table S5).[47,55]

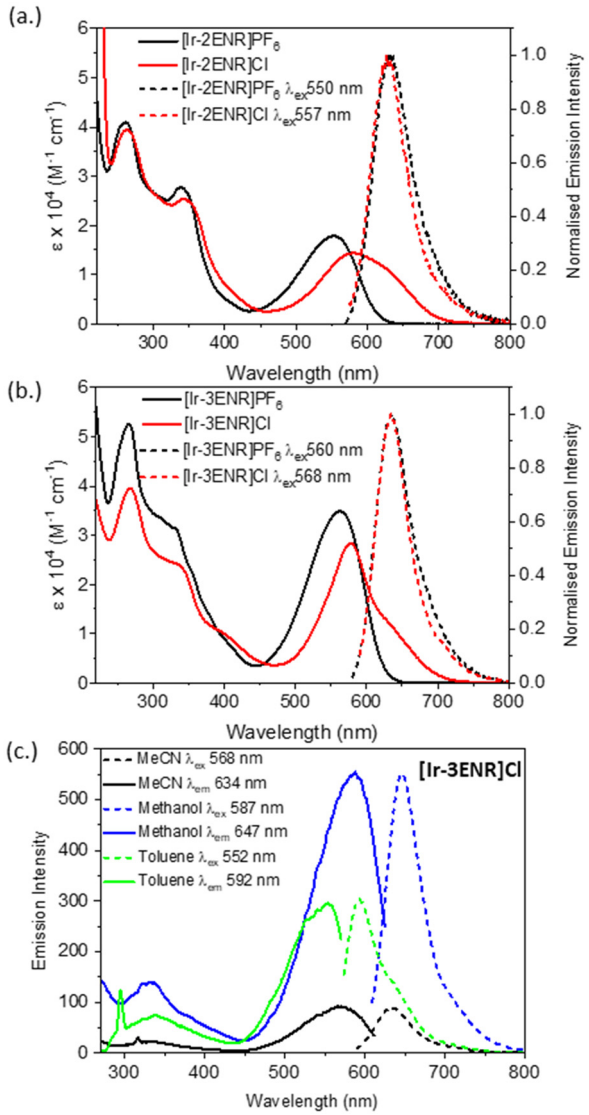

Fig. 1 (a) UV-Visible absorption (solid) and emission (dashed) spectra of (a) **[Ir-2ENR]PF_6/Cl** and (b) **[Ir-3ENR]PF_6/Cl** in MeCN, 298 K. (c) Excitation (solid) and emission (dashed) solvatochromism studies of **[Ir-3ENR]Cl** in MeCN, MeOH, and Toluene.

When exciting into the ^{1}CT absorption band (λ_{ex} 560 nm, MeCN) of **3ENR-bpy**, a featureless emission band centred at 635 nm is observed (Fig. S13b), which is assigned to a ^{1}CT* emission supported by the blue-shifted emission at low temperature measurements (Fig. S13c). The emission profile under inert atmosphere showed minimal changes confirming the fluorescent nature of the excited state and its singlet state origin (Fig. S13d). The short emission lifetime (τ_{em}, 4.04 ns), and the high quantum yield (Φ_{em}, 71.1%) further support this assignment.

For the Ir(III) complexes, excitation into either the ^{1}MLCT (λ_{ex} *circa* 340 nm) or into the ^{1}ILCT absorption bands, leads to emissions centred at around 630 nm in MeCN (Fig. 1a and b and Fig. S15). The profile of the emission spectra recorded

Table 1 Photophysical data of the generated complexes **[Ir-2ENR]PF_6/Cl**, **[Ir-3ENR]PF_6/Cl**, **[Ru-2ENR]$(PF_6)_2$** and **[Ru-3ENR]$(PF_6)_2$**, and the ligand **3ENR-bpy**

Compound	λ_{abs} [a] (nm)	ε [b] (10^4 M^{-1} cm^{-1})	λ_{ex} (nm)	λ_{em} [c] (nm)	Φ_{em} (%)	τ_{em} [f] (ns)	τ_T (μs)	Φ_Δ (%)
[Ir-2ENR]PF_6	260	4.10	550	630	2.4[d]	4.40[g]	97.3[j]	4.3[n]
	338	2.74					101.6[k]	4.0[o]
	553	1.78						
[Ir-3ENR]PF_6	265	5.28	560	635	4.8[d]	3.76[g]	125.4[j]	6.4[n]
	331	3.16					88.1[k]	9.7[o]
	562	3.48						
[Ir-2ENR]Cl	262	5.25	557	630	—	—	—	—
	339	3.59						
	567	2.83						
[Ir-3ENR]Cl	268	3.95	568	633			—	—
	578	2.82						
[Ru-2ENR]$(PF_6)_2$	450	1.19	450	640	2.4/0.6[e]	726.42[h]	123.4[l]	42.3[n]
	460	3.35	560	635	—/0.6[d]		140.2[m]	77.2[o]
[Ru-3ENR]$(PF_6)_2$	450	1.26	450	650	2.3/0.6[e]	1785.42[i]	206.0[l]	51.0[n]
	565	4.73	565	635	—/0.4[d]		234.7[m]	90.4[o]
3ENR-bpy	275	4.00	560	635	71.1[d]	—	—	—
	313	4.20						
	357	1.90						
	557	6.19						

[a] In MeCN [10^{-5} M], 298 K. [b] Molar extinction coefficient at the absorption maxima, MeCN [10^{-5} M], 298 K. [c] Emission maximum in degassed MeCN, excited at the corresponding λ_{ex} value. [d] Fluorescence quantum yield in Ar with Nile red as a standard (Φ_f 76% in MeCN).[57] [e] Phosphorescent quantum yield in Ar with $[Ru(bpy)_3](PF_6)_2$ as a standard (Φ_p 9.5% in MeCN).[57] [f] Emission lifetime (λ_{ex} 458 nm). [g] Fitted monoexponentially. [h] Fitted with a biexponential equation (268.97 × 43.31% + 1075.90 × 56.69%). [i] Fitted with a biexponential equation (784.80 × 57.50% + 3139.19 × 42.50%). [j] Triplet-state lifetime, in deaerated MeCN excited at 355 nm [10^{-5} M], 298 K. [k] Triplet-state lifetime, in deaerated MeCN excited at 550 nm [10^{-5} M], 298 K. [l] Triplet-state lifetime, in deaerated MeCN excited at 450 nm [10^{-5} M], 298 K. [m] Triplet-state lifetime, in deaerated MeCN excited at 565 nm [10^{-5} M], 298 K. [n] Singlet oxygen quantum yield (λ_{ex} 534 nm) with diiodobodipy as the standard (Φ_Δ 83% in CH_2Cl_2).[58] [o] Singlet oxygen quantum yield with methylene blue as the standard (Φ_Δ = 57% in CH_2Cl_2) in MeCN, λ_{ex} = 610 nm.

under inert atmosphere closely match that of **3ENR-bpy** and the ^{1}ILCT* emission bands for the previously reported Ru(II) analogues, **[Ru-2ENR]$(PF_6)_2$** and **[Ru-3ENR]$(PF_6)_2$**, therefore these are assigned as ^{1}ILCT-based emission.[47] Positive solvatochromism was observed in the emission spectra for the Ir(III) complexes, following the trend observed for Nile red and its derivatives (Fig. 1c and Fig. S13, S15).[56] Independent excitation into the ^{1}MLCT or the ^{1}ILCT bands leads to the same emission wavelengths for the two Ir(III) complexes in different solvents (Fig. S15e and f).

The emission spectra of **[Ir-2ENR]PF_6** and **[Ir-3ENR]PF_6** in aerated solutions showed (small 17 and 5% respectively) oxygen response when excited into the ^{1}MLCT (λ_{ex} 340 nm) and negligible response when the ^{1}ILCT (λ_{ex} 550/560 nm) was excited, again indicating the primarily singlet character of the excited state (Fig. S16a and b).

Hypsochromic shifts are observed upon cooling to 77 K, confirming the charge transfer nature of the observed emissions (Fig. S16c–f). Short emission lifetimes (τ_{em}), 4.40 ns (630 nm) for **[Ir-2ENR]PF_6** and 3.76 ns (635 nm) for **[Ir-3ENR]PF_6**, after 458 nm excitation, confirm fluorescence originating from the ^{1}ILCT transition.

The quantum yield of emission (Φ_{em}) was calculated using **NR** as a reference (Φ_{em} 76% in MeCN) and found to be 2.4% and 4.8% for **[Ir-2ENR]PF_6** and **[Ir-3ENR]PF_6** respectively (Table 1).

As for the Ru(II) analogues, the emission quantum yield indicates strongly quenched singlet fluorescence, due to incomplete $S_1 \rightarrow T_1$ ISC. This has been previously reported for Ir(III) complexes containing highly emissive chromophores like pyrene and rhodamine that are distant from the transition metal centre.[59,60]

Time-resolved spectroscopy

The time-resolved emission spectra after 510 nm laser excitation show a peak centred at 626 nm for **[Ir-2ENR]PF_6** and 633 nm for **[Ir-3ENR]PF_6** that decays within 4 ns indicative of singlet excited states and in support of the steady-state measurements (Fig. 2a and b).

Nanosecond time-resolved difference spectra reveal significant bleaching at *circa* 560 nm nm for **[Ir-2ENR]PF_6** and **[Ir-3ENR]PF_6** after exciting the ^{1}MLCT (355 nm) and the ^{1}ILCT bands (550 nm), due to the depletion of the ground state in the Nile red moiety (Fig. 2c and d and Fig. S17). The triplet excited state lifetimes (τ_T) at the bleaching peaks were 97.3/101.6 μs for **[Ir-2ENR]PF_6**, and 125.4/88.1 μs for **[Ir-3ENR]PF_6** (Table 1 and Fig. S18).

The long-lived triplet state lifetimes indicate a non-emissive ^{3}IL* or ^{3}ILCT* states as for the Ru(II) analogues previously supported by computational studies.[47] The diminished contribution from the metal centre results in very weak spin–orbit coupling to enable the triplet state to relax back to the ground state *via* ISC, and as the $T_1 \rightarrow S_0$ transition is strongly spin-forbidden it results in long-lived triplet state lifetimes.[61] The photophysical processes are depicted in a simplified Jablonski diagram (Scheme S1).

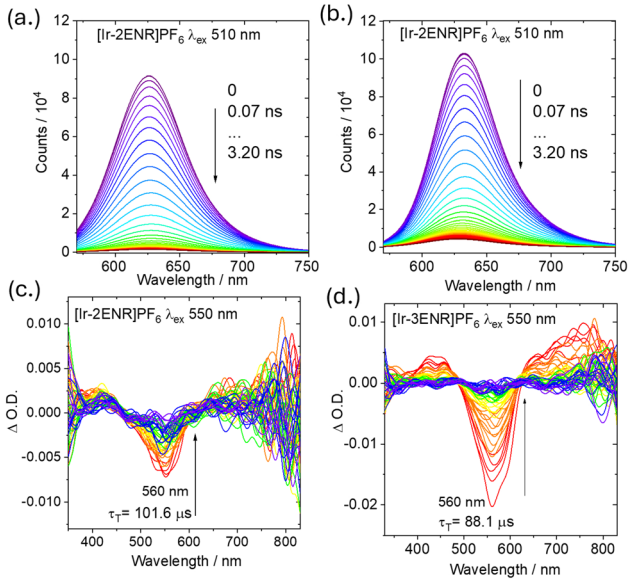

Fig. 2 Time-resolved emission spectra of (a) **[Ir-2ENR]PF$_6$** and (b) **[Ir-3ENR]PF$_6$**, λ_{ex} 510 nm, MeCN and of [10^{-5} M], 298 K. Nanosecond transient absorption spectra of (c) **[Ir-2ENR]PF$_6$** and (d) **[Ir-3ENR]PF$_6$** excited with nanosecond pulsed laser at 550 nm in deaerated MeCN and of [10^{-5} M], 298 K.

Singlet oxygen quantum yield

$^1O_2$ is a highly reactive, cytotoxic agent and has a central role in PDT, therefore it was important to determine the $^1O_2$ quantum yields (Φ_Δ) of the complexes. This was carried out *via* the relative spectroscopic method using 1,3-diphenylisobenzofuran (DPBF) as an $^1O_2$ scavenger, with diiodobodipy as the reference (83% in CH_2Cl_2) (Fig. S19 and S20).[58] **[Ir-2ENR]PF$_6$** and **[Ir-3ENR]PF$_6$** have low Φ_Δ, 4.3 and 6.4% respectively, compared to the two Ru(II) analogues which had Φ_Δ values of 42.3% and 51.0% (λ_{ex} 550 nm, MeCN). Liu *et al.* previously reported TM complexes having non-emissive rhodamine-based ^{3}IL states, which had Φ_Δ values inversely proportional to their related Φ_{em}.[60] The Ru(II) and Ir(III) NR complexes show a parallel trend, where **[Ir-3ENR]PF$_6$** had a Φ_{em} value over 10 times greater than its Ru(II) analogue (Φ_{em} 4.8% *versus* 0.4%), while its Φ_Δ was *circa* 10 times lower than **[Ru-3ENR](PF$_6$)$_2$** (6.4% *versus* 51.0%). Following the rhodamine family's example and explanation, the more efficient ISC led to lower residual fluorescence and lower Φ_{em} and simultaneously greater population of the NR-based 'dark' long-lived T_1* state that can generate $^1O_2$, resulting in higher Φ_Δ.

The Φ_Δ was remeasured using a longer excitation wavelength, λ_{ex} 610 nm, closer to the optimum therapeutic window for PDT (650–850 nm), using methylene blue as the standard (Φ_Δ 57% in CH_2Cl_2) (Fig. S20). There was a significant increase in Φ_Δ for **[Ir-3ENR]PF$_6$** (9.7%) while for **[Ir-2ENR]PF$_6$** (4.0%) the Φ_Δ remained the same. The data supports the fact that lower energy excitation is suitable to activate these compounds when considering them for PDT applications.

Biological studies with SKBR-3 cell line

The dark and phototoxicity of **[Ir-2ENR]Cl** and **[Ir-3ENR]Cl** were evaluated using the SKBR-3 cell line (a human breast cancer cell line) for comparison with the previously reported Ru(II) analogues. The two PSs were added at varying concentrations to determine the concentration at which at least 80% of the cells survive (Fig. 3a, b and Fig. S21). The PSs were incubated with the cells for 24 h, after which time, the cell viability was then tested with the Alamar Blue assay (24 h) followed by another 48 hours of incubation and cell viability testing (72 h) (Fig. 3a, b and Fig. S22). At 10 nM concentrations the cell viability was sufficient for the phototoxicity studies (Fig. 3a and b).

Phototoxicity of the complexes was determined by irradiating cells, incubated with the PSs for 4 h, with 630 nm (33 J cm^{-2}) light for 15 min. After irradiation, cell viability was tested immediately (4 h, Fig. 3c). The cells were then incubated in the dark for 48 h, after which time cell viability was tested again (52 h) (Fig. 3d). After 4 h, a 20% cell viability decrease was observed when incubated with **[Ir-2ENR]Cl** or **[Ir-3ENR]Cl**, however after a further 48 h incubation **[Ir-3ENR]Cl** killed *circa* 80% of the cells, surpassing the toxicity of the previously reported Ru(II) analogue that killed 60% of the cells at the same concentration. The two **3ENR**-bearing complexes showed increased Φ_Δ compared to their **2ENR** analogues, which explains the enhanced photodynamic action seen for **[Ru-3ENR]Cl$_2$** and **[Ir-3ENR]Cl**. **[Ir-3ENR]Cl** exhibited the highest potency 48 h after irradiation which was surprising as the Ru analogue had higher Φ_Δ.

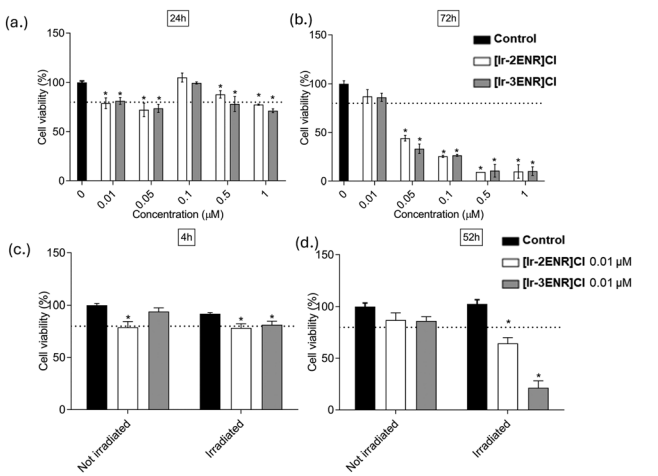

Fig. 3 Dark toxicity (a and b). Cell viability of SKBR-3 cells incubated in dark conditions with different concentrations of **[Ir-2ENR]Cl**, **[Ir-3ENR]Cl**, (0.01, 0.05, 0.1, 0.5 and 1 μM), and control (0 μM) at (a) 24 h and (b) 72 h. Photodynamic treatment effects after 15 min irradiation (c and d). Cell viability of SKBR-3 cells incubated without (control) or with 0.01 μM of **[Ir-2ENR]Cl** and **[Ir-3ENR]Cl** for 4 h followed by cell wash. Cell viability was determined immediately after incubation (c) (4 h) either in dark conditions (not irradiated) or after 15 min irradiation at λ_{ex} 620–630 nm (irradiated) and (d) after further 48 h in standard culture conditions (52 h). Experiments were carried out in triplicate. Asterisks indicate statistically significant differences in the cell viability between not irradiated control and product at each time-point and condition (*$p < 0.05$).

Product internalisation experiments performed *via* confocal imaging at a concentration of 10 μM showed that both Ir(III) complexes were internalised successfully (Fig. 4). The uniform distribution of the product within the cells confirmed that the PSs probably entered the cells *via* diffusion. If the product was taken up by the cells *via* endocytosis, the product would have been trapped in vesicles and would be seen as discrete dots and not diffused.

Phototoxicity studies showed that while having a lower Φ_Δ (λ_{ex} 610 nm, Φ_Δ 9.7%, PF_6 salt) **[Ir-3ENR]Cl** is more potent at killing cells after irradiation than **[Ru-3ENR]Cl_2** Φ_Δ (λ_{ex} 610 nm, Φ_Δ 90.4%, PF_6 salt). One of the factors contributing to this is that the Ir(III) complex is taken up by the cells much more efficiently, resulting in a higher concentration within the cells. It was also conceivable that the complex's toxicity stems from an oxygen-independent pathway (type-I and type III). Due to its improved cellular uptake and PDT behaviour, **[Ir-3ENR]Cl** was identified as the lead compound and further studies were carried out to investigate its mode of action.

Biological studies with MCF-7 cell line

The cyto- and photocytotoxicity of **[Ir-3ENR]Cl** were evaluated on the MCF-7 human breast adenocarcinoma cell line. The complex showed significant 'dark' cytotoxicity, presenting IC_{50} values in the low micromolar range after 24 h, and 72 h incubation, under normoxic conditions (O_2 21%) (Table 2). Prolongation of the incubation time from 24 h to 72 h only slightly increased the toxicity of the complex, demonstrating its efficient and quite fast accumulation. High levels of cellular uptake of the Ir(III) complex were confirmed by inductively coupled plasma mass spectrometry (ICP-MS), with accumulation in the MCF-7 cells exceeding 300-fold, compared to the cell medium. The cytotoxicity of the complex was retained under hypoxic (O_2 1%) conditions and had similar values to the normoxic at 24 h and 72 h. For the phototoxicity measurements, non-toxic concentrations of the Ir(III) complex were used to determine the PDT activity of the compounds on the MCF-7 cell line. The Nile red complex exhibited a significant increase in toxicity after 520 nm monochromatic light activation (5 min, 82 mJ cm^{-2}, 273.2 μW cm^{-2}) under normoxia, reducing the IC_{50} value to nanomolar levels (Table 2). Light activation amplified the toxicity, shown by the high phototherapeutic index (PI = 179), that was calculated as the ratio of 'dark' and irradiated IC_{50} values ($IC_{50}^{dark}/IC_{50}^{h\nu}$). The phototoxicity under hypoxia[62] (1%) was further increased by 5-fold, making the Ir(III) complex an excellent PDT agent, suitable to be used under decreased oxygen concentration ($HCR^{h\nu}$ $h\nu$ $IC_{50}^{hyp}/IC_{50}^{norm}$ = 0.176).

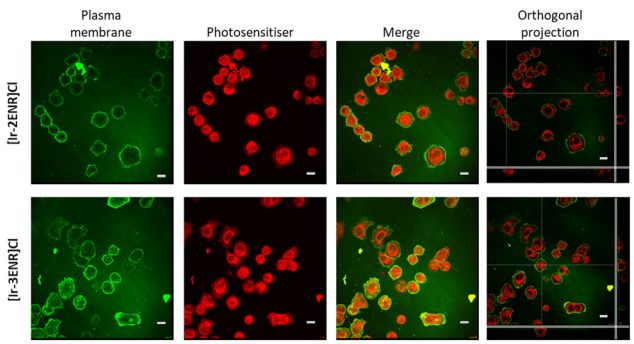

Fig. 4 Product internalisation. Live SKBR-3 cells incubated with 10 μM of **[Ir-2ENR]Cl** and **[Ir-3ENR]Cl**, for 4 h and observed under confocal microscope. To analyse the localisation of the product, fluorescence mode was used. Product fluorescence emission was detected in the range of λ_{em} 580–699 nm by exciting the cells using a λ_{ex} 488 nm laser (15% of laser power). Wheat germ agglutinin (WGA) fluorescence emission (membrane) was detected in the range of λ_{em} 500–530 nm (green) by exciting the cells using a λ_{ex} 488 nm laser (12% of laser power). Maximum projection and orthogonal projection of *z*-stacks. Scale bar 20 μm.

To explore where ROS are involved with the cytotoxicity and photocytotoxicity of the complex, *in vitro* ROS generation studies were carried out using different fluorescent probes.[63] After the incubation of MCF-7 cells with non-toxic concentrations of **[Ir-3ENR]Cl** (IC_{50}/4 and IC_{50}/2) in the dark, the fluorescent intensity of singlet oxygen sensor green (SOSG, sensitive towards singlet oxygen), hydroxyphenyl fluorescein (HPF, sensitive towards hydroxyl radical), 2′,7′-dichlorodihydrofluorescein diacetate (DCFDA, often used as total ROS indicator, but most sensitive towards H_2O_2), and hydroethidine (HE, used as $O_2^{\bullet-}$ probe) were measured (Fig. 5a). All used probes showed increased fluorescence intensity compared to the control, indicating high $^1O_2$, H_2O_2, $^{\bullet}OH$, and $O_2^{\bullet-}$ generation in a concentration-dependent manner. Mitochondrial superoxide production was also detected using MitoSox probe, which showed increased fluorescence after incubation with **[Ir3ENR]Cl** (Fig. 5a). A liposoluble peroxidation sensor, C11-BODIPY$^{581/591}$, was used to assess cell membrane damage. Lipid peroxyl radicals ($ROO^{\bullet}$) oxidise the probe and alter its fluorescence properties, switching its emission from red to green. Incubation of MCF-7 cells with **[Ir-3ENR]Cl** caused for-

Table 2 Dark- and light-activated cytotoxicity values (IC_{50}) against the MCF-7 line under normoxic (21% O_2) and hypoxic (1% O_2) conditions, cellular uptake (measured by ICP-MS as the ratio of the Ir accumulated in cells *vs.* Ir added to the medium), and calculated phototherapeutic index (PI = $IC_{50}^{dark}/IC_{50}^{h\nu}$) and hypoxic cytotoxicity ratio (HCR = $IC_{50}^{hyp}/IC_{50}^{norm}$) values for **[Ir-3ENR]Cl** determined against MCF-7 cell line

MCF-7 cell line	Time	IC_{50} [μM] normoxia	IC_{50} [μM] hypoxia	HCR	$IC_{50}^{h\nu}$ [nM] normoxia	$IC_{50}^{h\nu}$ [nM] hypoxia	$PI^{h\nu}$	$HCR^{h\nu}$	$\frac{[Ir_{cell}]}{[Ir_{medium}]}$
[Ir-3ENR]Cl	24 h	7.50 ± 3.35	6.83 ± 3.76	0.91	42.50 ± 12.58	7.47 ± 1.85	179	0.176	344
	72 h	1.07 ± 0.40	1.40 ± 0.33	1.31	—	—			

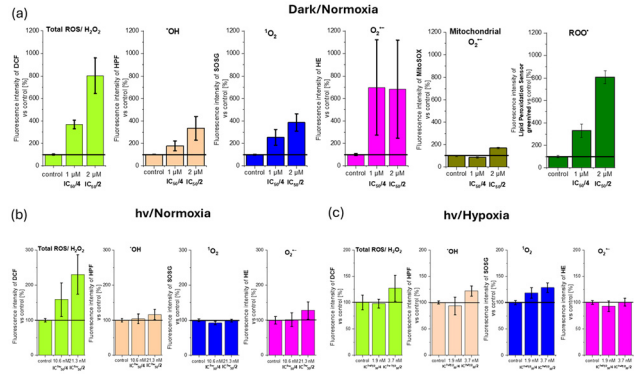

Fig. 5 The level of ROS measured by selective fluorescent probes induced in MCF-7 cells after 24 h treatment with **[Ir-3ENR]Cl**. (a) ROS production under normoxic conditions and without irradiation, (b) ROS production (H_2O_2, $^{\bullet}OH$, $^1O_2$ and $O_2^{\bullet-}$) under normoxia after irradiation and (c) ROS production under hypoxia and irradiation [DCF – 2′,7′-dichlorodihydrofluorescein diacetate (H_2O_2); HPF – hydroxyphenyl fluorescein ($^{\bullet}OH$, $ONOO^-$); SOSG – Singlet Oxygen Sensor Green ($^1O_2$); HE – hydroethidine ($O_2^{\bullet-}$); MitoSox™ ($O_2^{\bullet-}$ in mitochondria) and lipid peroxidation sensor C11-BODIPY $^{581/591}$ (ROO$^{\bullet}$)].

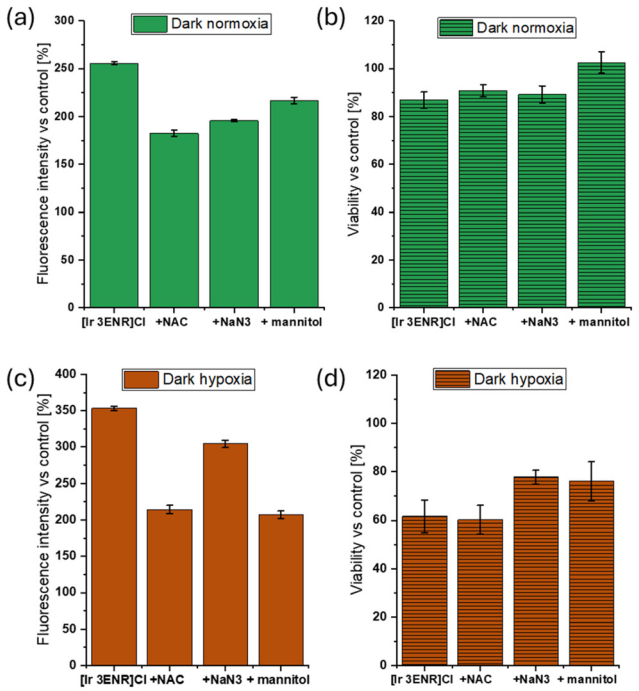

Fig. 6 ROS levels (a and c) and the viability (b and d) of MCF-7 cells after 24 h treatment with **[Ir-3ENR]Cl** (2 μM) without or with the antioxidants NAC (5 mM), NaN_3 (2 mM), or D-mannitol (50 mM) under normoxic (a and b) or hypoxic (c and d) conditions.

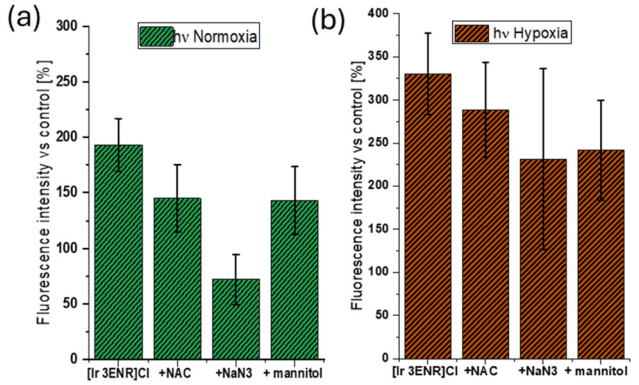

Fig. 7 ROS levels of MCF-7 cells after 24 h treatment with **[Ir-3ENR]Cl** (0.021 μM) without or with the antioxidants NAC (5 mM), NaN_3 (2 mM), or D-mannitol (50 mM) under normoxic (a) or hypoxic (b) conditions after irradiation (5 min, λ_{ex} 520 nm, 82 mJ cm^{-2}, 273.2 μW cm^{-2}).

mation of lipid peroxyl radicals, indicating cell membrane damage (Fig. 5a).

ROS generation under normoxic conditions after irradiation (5 min, λ_{ex} 520 nm, 82 mJ cm^{-2}, 273.2 μW cm^{-2}) was also explored using non-toxic concentrations of the compound ($IC_{50}{}^{h\nu}/4$ and $IC_{50}{}^{h\nu}/2$, 10.63 and 21.25 nM, respectively).

Irradiation amplified the ROS generation ability of the compound and revealed mainly elevated levels of H_2O_2, as well as a small increase in $^{\bullet}OH$, and $O_2^{\bullet-}$ production (Fig. 5b). Under hypoxic conditions at non-toxic low nanomolar concentration (hypoxic $IC_{50}{}^{h\nu}/4$, 1.86 nM and $IC_{50}{}^{h\nu}/2$, 3.74 nM) the compound still maintained its ability to increase ROS production following photoexcitation (Fig. 5c).

To verify the role of ROS in **[Ir-3ENR]Cl** triggered cytotoxicity, several ROS scavengers were employed. Cells were co-treated with a low concentration of *N*-acetylcysteine (NAC), a thiol-containing, broad-spectrum antioxidant and glutathione precursor;[64] sodium azide (NaN_3), a classical singlet oxygen scavenger;[65] or D-mannitol, a specific hydroxyl radical scavenger;[65] together with **[Ir-3ENR]Cl**. Co-treatment with these ROS scavengers inhibited the intracellular ROS generation induced by the complex (Fig. 6a and c) and, as expected, led to a reduction in the cytotoxic activity of **[Ir-3ENR]Cl** (Fig. 6b and d), as assessed by resazurin assay. Both mannitol and NaN_3 influenced ROS generation and **[Ir-3ENR]Cl** cytotoxicity, confirming engagement of ROS, type-I and II in the mechanism of cell death.

Co-treatment of cells with ROS scavengers reduced the ROS-generation ability of **[Ir-3ENR]Cl** even after irradiation (Fig. 7a and b), confirming that the phototoxicity activity of the Ir compound is based on both type I/II mechanisms. Although co-treatment with ROS scavengers significantly reduced intracellular ROS levels, cell viability following irradiation was not restored (Fig. S23). This indicates that ROS formation contributes to, but is not solely responsible for, the photocytotoxic effect of the Ir complex. Most likely, the observed cytotoxicity arises from additional ROS-independent photochemical mechanisms, including direct photoinduced electron transfer and organelle-localized photodamage, which are not efficiently mitigated by the antioxidant scavengers. This behaviour can be observed in mitochondria-localized Ir and Ru photosensitizers, where phototoxicity arises from rapid, localized mitochondrial damage and disruption of bioenergetic and redox homeostasis. Once mitochondrial integrity or respiratory function is compromised, downstream cell death pathways proceed

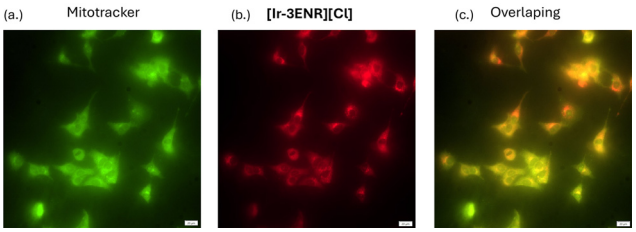

Fig. 8 Fluorescence images of MCF-7 cells showing subcellular localization of **[Ir-3ENR]Cl** (1 μM, incubation 24 h). (a) MitoTracker Green was used to image mitochondria, green colour arises from the organelle-specific dye, (b) red colour comes from **[Ir-3ENR]Cl** complex emission, (c) yellow colour represents overlap of the red luminescence of the complex and green emission from the dye indicating co-localization. Scale bars 20 μm.

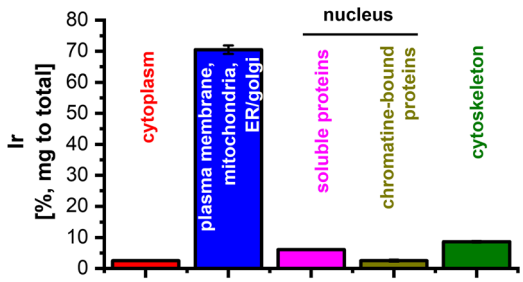

Fig. 9 ICP-MS analysis of the distinct cellular compartments of MCF-7 cells after 24 h treatment with 2 μM **[Ir-3ENR]Cl**.

irreversibly and cannot be suppressed by diffusible antioxidant scavengers.[65,66]

The subcellular localisation of **[Ir-3ENR]Cl** was assessed after exposure of the cells to the compound for 24 hours. For co-localization studies, cells were co-stained with the green-fluorescent dye MitoTracker™ (Thermofisher Scientific) and revealed that **[Ir-3ENR]Cl** accumulated in the mitochondria (Pearson correlation coefficient PCC = 0.852) (Fig. 8).

To further confirm the subcellular localization of **[Ir-3ENR]Cl**, subcellular fractionation was performed to isolate distinct cellular compartments. ICP-MS analysis of the resulting fractions confirmed that the **[Ir-3ENR]Cl** complex accumulated primarily in the fraction containing the plasma membrane, mitochondria, and ER/golgi structures (Fig. 9).

Conclusions

In summary, two novel Nile red containing Ir(III) bis-cyclometalated complexes were synthesised and fully characterised. Their spectroscopic and photophysical properties were investigated by steady-state and time-resolved absorption and emission spectroscopy. The results indicate the presence of a low energy non-emissive ^{3}ILCT state located on the NR moiety, that is beneficial for the potential PDT activity.

Despite the lower singlet oxygen quantum yield of **[Ir-3ENR]Cl**, biological studies conducted with SKBR-3 cells revealed that this Ir(III) compound possesses excellent phototoxic activity. This has been observed recently in bipyridyl Ru(II) and Ir(III) complexes containing coumarin which similarly have relatively low singlet oxygen yields, yet perform well under normoxic and hypoxic conditions as type I/II PDT agents.[67,68] As in the former case, we propose that under hypoxia the electron transfer pathway takes over with superoxide behaving as an electron donor.[68]

The cyclometalated Ir(III) frame led to excellent cellular uptake in both SKBR-3 and MCF-7 cell lines due to the increased lipophilicity.

The photodynamic activity of **[Ir-3ENR]Cl** was further investigated on MCF-7 cells, including normoxic and hypoxic phototoxicity, scavenger assay, accumulation, localisation and *in vitro* ROS generation studies. The results show that the Ir(III) Nile red complex demonstrated hypoxia-tolerant type I and II photodynamic behaviour, efficiently generating H_2O_2, $OH^{\bullet}$, $^1O_2$ and $O_2^{\bullet-}$ even at extremely low concentrations (3.74 nM) under decreased oxygen concentration. The complex localised in mitochondria and disturbed their function as evidenced by increased mitochondrial superoxide production. **[Ir-3ENR]Cl** appeared to be an extremely efficient photosensitizer and has a high phototoxicity index (PI = 179). Furthermore, its phototoxicity increased five-fold under hypoxia, making it an excellent fluorescent PDT agent, with light activation beneficially in the green/red region with promising applications in diagnostics and the PDT treatment of hypoxic tumours. Increase of the photodynamic effect under decreased oxygen concentration suggests that **[Ir-3ENR]Cl** exerts its phototoxicity *via* both oxygen-independent and oxygen-dependent mechanisms.

Conflicts of interest

There are no conflicts to declare.

Data availability

The data supporting this article have been included as part of the supplementary information (SI). Supplementary information: experimental details and synthetic methods; high resolution mass spectral data (Table S1); NMR data for the ligand and novel complexes (Fig. S1–S9); electrochemical cyclic voltammograms (Fig. S10–S12 and Table S2); photophysical spectra (Fig. S13–S16 and Tables S3–S5); transient nanosecond absorption spectra (Fig. S17 and S18); singlet oxygen quantum yield measurements (Fig. S19 and S20); dark toxicity data and biological method (Fig. S21–S23). See DOI: **https://doi.org/10.1039/d6qi00188b**.

Acknowledgements

This publication has emanated from research conducted with the financial support of Science Foundation Ireland (Grant Number 15/IA/3046), and Research Ireland (Grant Number 12/

RC/2278_2) which is co-funded under the European Regional Development Fund under the AMBER award. A. Al-R. acknowledges funding from a TCD Postgraduate Studentship 1252 Award. J. F. acknowledges funding support from the Trinity Research Doctoral Higher Education Authority and the Department of Further and Higher Education, Research, Innovation and Science and Royal Society of Chemistry Researcher Collaboration Grant (C23-5428184643). O. M. acknowledges the support from the "Excellence Initiative – Research University" program at the Jagiellonian University in Kraków. The graphical abstract was created in BioRender (J. Fodor 2026) **https://BioRender.com/yiwve6b**.

References

1 T. J. Dougherty and S. L. Marcus, Photodynamic therapy, *Eur. J. Cancer*, 1992, **28**, 1734–1742.
2 T. C. Pham, V.-N. Nguyen, Y. Choi, S. Lee and J. Yoon, Recent Strategies to Develop Innovative Photosensitizers for Enhanced Photodynamic Therapy, *Chem. Rev.*, 2021, **121**, 13454–13619.
3 K. Gollnick, in *Advances in Photochemistry*, 1968, pp. 1–122, DOI: **10.1002/9780470133361.ch1**.
4 G. O. Schenck, Photosensitization, *Ind. Eng. Chem.*, 1963, **55**, 40–43.
5 C. S. Foote, Definition of type I and type II photosensitized oxidation, *Photochem. Photobiol.*, 1991, **54**, 659.
6 O. Mazuryk, E. Janczy-Cempa, J. Łagosz, D. Rutkowska-Zbik, A. Machnicka, A. Krasowska, P. Pietrzyk, G. Stochel and M. Brindell, Relevance of the electron transfer pathway in photodynamic activity of Ru(ii) polypyridyl complexes containing 4,7-diphenyl-1,10-phenanthroline ligands under normoxic and hypoxic conditions, *Dalton Trans.*, 2022, **51**, 1888–1900.
7 J. Jiang, X. Lv, H. Cheng, D. Yang, W. Xu, Y. Hu, Y. Song and G. Zeng, Type I photodynamic antimicrobial therapy: Principles, progress, and future perspectives, *Acta Biomater.*, 2024, **177**, 1–19.
8 H. Mattila, S. Khorobrykh, V. Havurinne and E. Tyystjärvi, Reactive oxygen species: Reactions and detection from photosynthetic tissues, *J. Photochem. Photobiol., B*, 2015, **152**, 176–214.
9 D. Chen, Q. Xu, W. Wang, J. Shao, W. Huang and X. Dong, Type I Photosensitizers Revitalizing Photodynamic Oncotherapy, *Small*, 2021, **17**, 2006742.
10 Y.-Y. Wang, Y.-C. Liu, H. Sun and D.-S. Guo, Type I photodynamic therapy by organic–inorganic hybrid materials: From strategies to applications, *Coord. Chem. Rev.*, 2019, **395**, 46–62.
11 Q. Yao, J. Fan, S. Long, X. Zhao, H. Li, J. Du, K. Shao and X. Peng, The concept and examples of type-III photosensitizers for cancer photodynamic therapy, *Chem*, 2022, **8**, 197–209.
12 Z. Chen, J. Xue, T. Zhang, W. Lv, X. Hu, Y. Xu and Q. Zhao, Engineering iridium(III) complexes for enhancing electron transfer-based photodynamic therapy, *Coord. Chem. Rev.*, 2026, **560**, 217877.
13 M. Li, J. Xiong, Y. Zhang, L. Yu, L. Yue, C. Yoon, Y. Kim, Y. Zhou, X. Chen, Y. Xu, X. Peng and J. S. Kim, New guidelines and definitions for type I photodynamic therapy, *Chem. Soc. Rev.*, 2025, **54**, 7025–7057.
14 C. Lu, W. Xu, H. Shah, B. Liu, W. Xu, L. Sun, S. Y. Qian and W. Sun, In Vitro Photodynamic Therapy of Mononuclear and Dinuclear Iridium(III) Bis(terpyridine) Complexes, *ACS Appl. Bio Mater.*, 2020, **3**, 6865–6875.
15 J. Sanz-Villafruela, C. Bermejo-Casadesus, E. Zafon, M. Martínez-Alonso, G. Durá, A. Heras, I. Soriano-Díaz, A. Giussani, E. Ortí, F. Tebar, G. Espino and A. Massaguer, Insights into the anticancer photodynamic activity of Ir(III) and Ru(II) polypyridyl complexes bearing β-carboline ligands, *Eur. J. Med. Chem.*, 2024, **276**, 116618.
16 J. Pracharova, G. Vigueras, V. Novohradsky, N. Cutillas, C. Janiak, H. Kostrhunova, J. Kasparkova, J. Ruiz and V. Brabec, Exploring the Effect of Polypyridyl Ligands on the Anticancer Activity of Phosphorescent Iridium(III) Complexes: From Proteosynthesis Inhibitors to Photodynamic Therapy Agents, *Chem. – Eur. J.*, 2018, **24**, 4607–4619.
17 H. Huang, S. Banerjee and P. J. Sadler, Recent Advances in the Design of Targeted Iridium(III) Photosensitizers for Photodynamic Therapy, *ChemBioChem*, 2018, **19**, 1574–1589.
18 X.-L. Li, L.-Z. Zeng, R. Yang, X.-D. Bi, Y. Zhang, R.-B. Cui, X.-X. Wu and F. Gao, Iridium(III)-Based Infrared Two-Photon Photosensitizers: Systematic Regulation of Their Photodynamic Therapy Efficacy, *Inorg. Chem.*, 2023, **62**, 16122–16130.
19 X.-D. Bi, R. Yang, Y.-C. Zhou, D. Chen, G.-K. Li, Y.-X. Guo, M.-F. Wang, D. Liu and F. Gao, Cyclometalated Iridium(III) Complexes as High-Sensitivity Two-Photon Excited Mitochondria Dyes and Near-Infrared Photodynamic Therapy Agents, *Inorg. Chem.*, 2020, **59**, 14920–14931.
20 E. Zafon, I. Echevarría, S. Barrabés, B. R. Manzano, F. A. Jalón, A. M. Rodríguez, A. Massaguer and G. Espino, Photodynamic therapy with mitochondria-targeted biscyclometallated Ir(III) complexes. Multi-action mechanism and strong influence of the cyclometallating ligand, *Dalton Trans.*, 2022, **51**, 111–128.
21 H. Huang, S. Banerjee, K. Qiu, P. Zhang, O. Blacque, T. Malcomson, M. J. Paterson, G. J. Clarkson, M. Staniforth, V. G. Stavros, G. Gasser, H. Chao and P. J. Sadler, Targeted photoredox catalysis in cancer cells, *Nat. Chem.*, 2019, **11**, 1041–1048.
22 X.-D. Song, B.-B. Chen, S.-F. He, N.-L. Pan, J.-X. Liao, J.-X. Chen, G.-H. Wang and J. Sun, Guanidine-modified cyclometalated iridium(III) complexes for mitochondria-targeted imaging and photodynamic therapy, *Eur. J. Med. Chem.*, 2019, **179**, 26–37.
23 D. E. J. G. J. Dolmans, D. Fukumura and R. K. Jain, Photodynamic therapy for cancer, *Nat. Rev. Cancer*, 2003, **3**, 380–387.

24 L. Luo, T. Zhu, X. Lu, B. Li, Q. Zhang, D. Li, J. Wu, Y. Tian, S. Ma and X. Tian, Optical modulation of Iridium(III) complexes for enhanced ROS generation: Multi-photon absorption and near-infrared photodynamic therapy insights, *Dyes Pigm.*, 2024, **221**, 111773.

25 S. Kuang, F. Wei, J. Karges, L. Ke, K. Xiong, X. Liao, G. Gasser, L. Ji and H. Chao, Photodecaging of a Mitochondria-Localized Iridium(III) Endoperoxide Complex for Two-Photon Photoactivated Therapy under Hypoxia, *J. Am. Chem. Soc.*, 2022, **144**, 4091–4101.

26 J. Sanz-Villafruela, C. Bermejo-Casadesús, G. Riesco-Llach, M. Iglesias, M. Martínez-Alonso, M. Planas, L. Feliu, G. Espino and A. Massaguer, Bombesin-Targeted Delivery of β-Carboline-Based Ir(III) and Ru(II) Photosensitizers for a Selective Photodynamic Therapy of Prostate Cancer, *Inorg. Chem.*, 2024, **63**, 19140–19155.

27 M. Negi, T. Dixit and V. Venkatesh, Ligand Dictated Photosensitization of Iridium(III) Dithiocarbamate Complexes for Photodynamic Therapy, *Inorg. Chem.*, 2023, **62**, 20080–20095.

28 J. Sanz-Villafruela, C. Bermejo-Casadesús, M. Martínez-Alonso, A. Moro, J. C. Lima, A. Massaguer and G. Espino, Towards efficient Ir(iii) anticancer photodynamic therapy agents by extending π-conjugation on N^N ligands, *Dalton Trans.*, 2024, **53**, 11393–11409.

29 W. Chen, Q. Zheng, W. Zhang, F. Fu and M.-J. Li, Mitochondria-Localized and Aggregation-Induced Near-Infrared Emission Iridium(III) Complexes for Photodynamic Therapy, *Inorg. Chem.*, 2025, **64**, 14487–14497.

30 R. Bevernaegie, B. Doix, E. Bastien, A. Diman, A. Decottignies, O. Feron and B. Elias, Exploring the Phototoxicity of Hypoxic Active Iridium(III)-Based Sensitizers in 3D Tumor Spheroids, *J. Am. Chem. Soc.*, 2019, **141**, 18486–18491.

31 Z. Lv, H. Wei, Q. Li, X. Su, S. Liu, K. Y. Zhang, W. Lv, Q. Zhao, X. Li and W. Huang, Achieving efficient photodynamic therapy under both normoxia and hypoxia using cyclometalated Ru(II) photosensitizer through type I photochemical process, *Chem. Sci.*, 2018, **9**, 502–512.

32 Z. Tan, J. Feng, Z. Tang, T. Feng, T. Liu, Y. Zhao and H. Chao, Iridium(III) complexes as type I photosensitizers for hypoxic two-photon photodynamic therapy, *J. Inorg. Biochem.*, 2025, **272**, 113006.

33 Y. Lu, R. Conway-Kenny, B. Twamley, N. McGoldrick, J. Zhao and S. M. Draper, 1,10-Phenanthroline Ruthenium(II) Complexes as Model Systems in the Search for High-Performing Triplet Photosensitisers: Addressing Ligand versus Metal Effects, *ChemPhotoChem*, 2017, **1**, 544–552.

34 L. Hallen, A. M. Horan, B. Twamley, E. M. McGarrigle and S. M. Draper, Accessing unsymmetrical Ru(ii) bipyridine complexes: a versatile synthetic mechanism for fine tuning photophysical properties, *Chem. Commun.*, 2023, **59**, 330–333.

35 L. Wei, R. Kushwaha, A. Dao, Z. Fan, S. Banerjee and H. Huang, Axisymmetric bis-tridentate Ir(iii) photoredox catalysts for anticancer phototherapy under hypoxia, *Chem. Commun.*, 2023, **59**, 3083–3086.

36 C. Gonzalo-Navarro, E. Zafon, J. A. Organero, F. A. Jalón, J. C. Lima, G. Espino, A. M. Rodríguez, L. Santos, A. J. Moro, S. Barrabés, J. Castro, J. Camacho-Aguayo, A. Massaguer, B. R. Manzano and G. Durá, Ir(III) Half-Sandwich Photosensitizers with a π-Expansive Ligand for Efficient Anticancer Photodynamic Therapy, *J. Med. Chem.*, 2024, **67**, 1783–1811.

37 J. Kasparkova, A. Hernández-García, H. Kostrhunova, M. Goicuría, V. Novohradsky, D. Bautista, L. Markova, M. D. Santana, V. Brabec and J. Ruiz, Novel 2-(5-Arylthiophen-2-yl)-benzoazole Cyclometalated Iridium(III) dppz Complexes Exhibit Selective Phototoxicity in Cancer Cells by Lysosomal Damage and Oncosis, *J. Med. Chem.*, 2024, **67**, 691–708.

38 V. Novohradsky, G. Vigueras, J. Pracharova, N. Cutillas, C. Janiak, H. Kostrhunova, V. Brabec, J. Ruiz and J. Kasparkova, Molecular superoxide radical photogeneration in cancer cells by dipyridophenazine iridium(III) complexes, *Inorg. Chem. Front.*, 2019, **6**, 2500–2513.

39 M. Redrado, A. Benedi, I. Marzo, M. C. Gimeno and V. Fernández-Moreira, Dual Emissive Ir(III) Complexes for Photodynamic Therapy and Bioimaging, *Pharmaceutics*, 2021, **13**, 1382.

40 B. Liu, S. Monro, Z. Li, M. A. Jabed, D. Ramirez, C. G. Cameron, K. Colón, J. Roque III, S. Kilina, J. Tian, S. A. McFarland and W. Sun, New Class of Homoleptic and Heteroleptic Bis(terpyridine) Iridium(III) Complexes with Strong Photodynamic Therapy Effects, *ACS Appl. Bio Mater.*, 2019, **2**, 2964–2977.

41 R. Conway-Kenny, A. Ferrer-Ugalde, O. Careta, X. Cui, J. Zhao, C. Nogués, R. Núñez, J. Cabrera-González and S. M. Draper, Ru(II) and Ir(III) phenanthroline-based photosensitisers bearing o-carborane: PDT agents with boron carriers for potential BNCT, *Biomater. Sci.*, 2021, **9**, 5691–5702.

42 J. Cabrera-González, J. Soriano, R. Conway-Kenny, J. Wang, Y. Lu, J. Zhao, C. Nogués and S. M. Draper, Multinuclear Ru(II) and Ir(III) decorated tetraphenylporphyrins as efficient PDT agents, *Biomater. Sci.*, 2019, **7**, 3287–3296.

43 Y. Lu, R. Conway-Kenny, J. Wang, X. Cui, J. Zhao and S. M. Draper, Exploiting coumarin-6 as ancillary ligands in 1,10-phenanthroline Ir(iii) complexes: generating triplet photosensitisers with high upconversion capabilities, *Dalton Trans.*, 2018, **47**, 8585–8589.

44 Y. Lu, J. Wang, N. McGoldrick, X. Cui, J. Zhao, C. Caverly, B. Twamley, G.MÓ. Máille, B. Irwin, R. Conway-Kenny and S. M. Draper, Iridium(III) Complexes Bearing Pyrene-Functionalized 1,10-Phenanthroline Ligands as Highly Efficient Sensitizers for Triplet-Triplet Annihilation Upconversion, *Angew. Chem., Int. Ed.*, 2016, **55**, 14688–14692.

45 J. Wang, Y. Lu, W. McCarthy, R. Conway-Kenny, B. Twamley, J. Zhao and S. M. Draper, Novel ruthenium and iridium complexes of N-substituted carbazole as triplet photosensitisers, *Chem. Commun.*, 2018, **54**, 1073–1076.

46 J. Wang, Y. Lu, N. McGoldrick, C. Zhang, W. Yang, J. Zhao and S. M. Draper, Dual phosphorescent dinuclear transition metal complexes, and their application as triplet photosensitizers for TTA upconversion and photodynamic therapy, *J. Mater. Chem. C*, 2016, **4**, 6131–6139.

47 C. Condon, R. Conway-Kenny, X. Cui, L. J. Hallen, B. Twamley, J. Zhao, G. W. Watson and S. M. Draper, Exploring the dark: detecting long-lived Nile Red 3ILCT states in Ru(ii) polypyridyl photosensitisers, *J. Mater. Chem. C*, 2021, **9**, 14573–14577.

48 C. Condon, O. Careta-Borràs, J. Fodor, A. B. Al Riyami, X. Xiao, J. Zhao, C. Nogués and S. M. Draper, Preliminary investigation of Ru(II) complexes bearing nile red chromophores for photodynamic therapy, *Front. Chem. Biol.*, 2025, **4**, 1620562.

49 F. Mohajer, M. M. Heravi, V. Zadsirjan and N. Poormohammad, Copper-free Sonogashira cross-coupling reactions: an overview, *RSC Adv.*, 2021, **11**, 6885–6925.

50 S. Lamansky, P. Djurovich, D. Murphy, F. Abdel-Razzaq, H.-E. Lee, C. Adachi, P. E. Burrows, S. R. Forrest and M. E. Thompson, Highly Phosphorescent Bis-Cyclometalated Iridium Complexes: Synthesis, Photophysical Characterization, and Use in Organic Light Emitting Diodes, *J. Am. Chem. Soc.*, 2001, **123**, 4304–4312.

51 M. S. Lowry, W. R. Hudson, R. A. Pascal and S. Bernhard, Accelerated Luminophore Discovery through Combinatorial Synthesis, *J. Am. Chem. Soc.*, 2004, **126**, 14129–14135.

52 E. Marchi, M. Locritani, M. Baroncini, G. Bergamini, R. Sinisi, M. Monari, C. Botta, W. Mróz, M. Bandini, P. Ceroni and V. Balzani, Blue and highly emitting [Ir(iv)] complexes by an efficient photoreaction of yellow luminescent [Ir(iii)] complexes, *J. Mater. Chem. C*, 2014, **2**, 4461–4467.

53 J. Sun, W. Wu, H. Guo and J. Zhao, Visible-Light Harvesting with Cyclometalated Iridium(III) Complexes Having Long-Lived 3IL Excited States and Their Application in Triplet–Triplet-Annihilation Based Upconversion, *Eur. J. Inorg. Chem.*, 2011, 3165–3173.

54 K. Hasan, A. K. Bansal, I. D. Samuel, C. Roldán-Carmona, H. J. Bolink and E. Zysman-Colman, Tuning the Emission of Cationic Iridium(III) Complexes Towards the Red Through Methoxy Substitution of the Cyclometalating Ligand, *Sci. Rep.*, 2015, **5**, 12325.

55 G. E. Schneider, H. J. Bolink, E. C. Constable, C. D. Ertl, C. E. Housecroft, A. Pertegàs, J. A. Zampese, A. Kanitz, F. Kessler and S. B. Meier, Chloride ion impact on materials for light-emitting electrochemical cells, *Dalton Trans.*, 2014, **43**, 1961–1964.

56 C. Gajo, D. Shchepanovska, J. F. Jones, G. Karras, P. Malakar, G. M. Greetham, O. A. Hawkins, C. J. C. Jordan, B. F. E. Curchod and T. A. A. Oliver, Nile Red Fluorescence: Where's the Twist?, *J. Phys. Chem. B*, 2024, **128**, 11768–11775.

57 A. Cser, K. Nagy and L. Biczók, Fluorescence lifetime of Nile Red as a probe for the hydrogen bonding strength with its microenvironment, *Chem. Phys. Lett.*, 2002, **360**, 473–478.

58 S. Ji, J. Ge, D. Escudero, Z. Wang, J. Zhao and D. Jacquemin, Molecular Structure–Intersystem Crossing Relationship of Heavy-Atom-Free BODIPY Triplet Photosensitizers, *J. Org. Chem.*, 2015, **80**, 5958–5963.

59 S. K. Seth and P. Purkayastha, Unusually Large Singlet Oxygen (1O2) Production by Very Weakly Emissive Pyrene-Functionalized Iridium(III) Complex: Interplay between Excited 3ILCT/3IL and 3MLCT States, *Eur. J. Inorg. Chem.*, 2020, 2990–2997.

60 C. Liu, L. Zhou, F. Wei, L. Li, S. Zhao, P. Gong, L. Cai and K. M.-C. Wong, Versatile Strategy To Generate a Rhodamine Triplet State as Mitochondria-Targeting Visible-Light Photosensitizers for Efficient Photodynamic Therapy, *ACS Appl. Mater. Interfaces*, 2019, **11**, 8797–8806.

61 C. Condon, PhD, Trinity College Dublin, 2023.

62 S. R. McKeown, Defining normoxia, physoxia and hypoxia in tumours-implications for treatment response, *Br. J. Radiol.*, 2014, **87**, 20130676.

63 M. Garcia-Diaz, Y.-Y. Huang and M. R. Hamblin, Use of fluorescent probes for ROS to tease apart Type I and Type II photochemical pathways in photodynamic therapy, *Methods*, 2016, **109**, 158–166.

64 R. A. De Grandis, K. M. Oliveira, A. P. M. Guedes, P. W. S. dos Santos, A. F. Aissa, A. A. Batista and F. R. Pavan, A Novel Ruthenium(II) Complex With Lapachol Induces G2/M Phase Arrest Through Aurora-B Kinase Down-Regulation and ROS-Mediated Apoptosis in Human Prostate Adenocarcinoma Cells, *Front. Oncol.*, 2021, **11**, 682968.

65 A. P. Castano, T. N. Demidova and M. R. Hamblin, Mechanisms in photodynamic therapy: Part two - Cellular signaling, cell metabolism and modes of cell death, *Photodiagnosis Photodyn. Ther.*, 2005, **2**, 1–23.

66 T. Feng, Z. Tang, J. Karges, J. Shu, K. Xiong, C. Jin, Y. Chen, G. Gasser, L. Ji and H. Chao, An iridium(III)-based photosensitizer disrupting the mitochondrial respiratory chain induces ferritinophagy-mediated immunogenic cell death, *Chem. Sci.*, 2024, **15**, 6752–6762.

67 E. Ortega-Forte, A. Rovira, P. Ashoo, E. Izquierdo-García, C. Hally, D. Abad-Montero, M. Jordà-Redondo, G. Vigueras, A. Deyà, J. L. Hernández, J. Galino, M. Bosch, M. E. Alberto, A. Francés-Monerris, S. Nonell, J. Ruiz and V. Marchán, Achieving red-light anticancer photodynamic therapy under hypoxia using Ir(III)–COUPY conjugates, *Inorg. Chem. Front.*, 2025, **12**, 3367–3383.

68 D. Abad-Montero, A. Gandioso, E. Izquierdo-García, S. Chumillas, A. Rovira, M. Bosch, M. Jordà-Redondo, D. Castaño, J. Bonelli, V. V. Novikov, A. Deyà, J. L. Hernández, J. Galino, M. E. Alberto, A. Francés-Monerris, S. Nonell, G. Gasser and V. Marchán, Ruthenium(II) Polypyridyl Complexes Containing COUBPY Ligands as Potent Photosensitizers for the Efficient Phototherapy of Hypoxic Tumors, *J. Am. Chem. Soc.*, 2025, **147**, 7360–7376.